

©2016

Tianya Yin

ALL RIGHTS RESERVED

Mathematical model and simulation study on the motion of suspended particles in 3D

deterministic lateral displacement

By

TIANYA YIN

A thesis submitted to

the Graduate School-New Brunswick

Rutgers, The State University of New Jersey

In partial fulfillment of the requirements

For the degree of

Master of Science

Graduate Program in Chemical and Biochemical Engineering

Written under the direction of

German Drazer

And approved by

New Brunswick, New Jersey

JANUARY, 2016

ABSTRACT OF THE THESIS

Mathematical model and simulation study on the motion of suspended particles in 3D
deterministic lateral displacement

by TIANYA YIN

Thesis Director:

German Drazer

Deterministic lateral displacement (DLD) is a size-based separation technique in microfluidic devices: as a suspension flows through a periodic array of posts, particles of different size migrate in different directions. In previous DLD systems, particles were confined to move in a plane perpendicular to the array of posts. Here, we present a 3D separation model in which the particles are driven by a constant force that not only has components in the plane perpendicular to the posts but also along them and, as a result, can generate both lateral (in-plane) and longitudinal (out-of-plane) displacements. Different models are studied to better understand the potential separation ability of this 3D system. We also present three dimensional simulations of a suspended particle driven by a constant force moving past a 3D array of posts. We find that the projection of particle trajectory on the perpendicular plane of posts shows directional locking analogous to the 2D case and the maximum value of longitudinal displacements per post are found near the transition angles at which the locking direction changes. We also identify driving angles that can separate particles taking advantage of both lateral and longitudinal displacements simultaneously.

Acknowledgement

I would never be able to finish my master's thesis without the guidance of my committee members, help from friends, and support from my family.

I would like to express my deepest gratitude to my advisor, Dr. German Drazer for his professional guidance and support of my study and research. His patience, motivation, and immense knowledge help and encourage me to overcome a lot of problems I met during my research. I would like to thank my committee members Dr. Shahab Shojaei-Zadeh and Dr. Gerardo Callegari for their interest in my work.

This work would not have been possible without the help of Peter Balogh who provides and revises the simulation code to me.

My sincere thanks to all my friends who supported me during my time in US. I am grateful for the help from Siqi who offers me numerous ideas and discussions on my research all the time. I especially appreciate Siqi, Ting, Zhanjie, Yanjun, David and Robert who make me a colorful graduate life at Rutgers.

Last but not the least, I would like to thank my parents for their continuous supporting me spiritually and materially throughout my life.

Table of Contents

Abstract of the Thesis	ii
Acknowledgement	iii
List of Illustrations	v
List of Tables.....	vi
1. Introduction.....	1
2. Numerical Method and Analytical Model.....	10
2.1 Objective	10
2.2 Nitsche's model ²⁶	11
2.3 Point-particle model.....	15
2.3.1 Single obstacle	15
2.3.2 Multiple obstacles	18
2.4 Simulation method.....	20
2.4.1 Single obstacle	21
2.4.2 Multiple obstacles	22
3. Results and discussions for single obstacle	24
3.1 Forcing direction angles from 2D to 3D	24
3.2 Results from different models for single obstacle	24
3.2.1 Nitsche's model	24
3.2.2 Simulation.....	26
3.2.3 Comparison of three models	27
4. Results in an array.....	30
4.1 Results, transition, displacement in y (Point-particle model).....	30
4.2 Comparison of point particle model with experiments.....	33
4.3 Comparison of point particle model with simulation	39
4.4 Triple separation	42
5. Conclusions.....	44
Reference	45

List of Illustrations

- Figure 1. Image of micro-particles migrating in the first generation DLD by Huang showing two types of trajectories: zigzag mode for particle radius of $0.4 \mu\text{m}$ (green trajectory) and displacement mode for particle radius of $1.0 \mu\text{m}$ (red trajectory). Image reproduced from Huang et al⁹. 2
- Figure 2. Schematic view of particle trajectories passing through a square periodic array of posts at two different forcing direction, where forcing angle α is an angle between driving field F and a column in the array (x axis), migration angle is β line L with respect to x axis. 4
- Figure 3. Particle trajectories showing directional locking with forcing direction ranging from 0 to 45° . Results are from Stokesian dynamics simulation and $[1,0]$, $[3,1]$, $[1,1]$, $[2,3]$ and $[1,2]$ represents different periodicity of particle trajectories in locked mode. 5
- Figure 4. (a) Schematic view of two types of particle trajectories resulting from hydrodynamic collision (when $b_{in} > b_c$, then $b_{out} = b_{in}$) and non-hydrodynamic collision (when $b_{in} \leq b_c$, then $b_{out} = b_c$). (Reproduced from Balvin et al.²¹); (b) Point particle model of two dimensional case (Reproduced from Risbud and Drazer²⁵) 7
- Figure 5. Schematic view of the forcing direction of particle exactly at the critical angle. In the second collision of particle with obstacle, the particle collides on the centerline of the obstacle, where critical offset b_c is the vertical distance between the centerlines of two obstacles. 8
- Figure 6. 3D-DLD on lateral displacement and longitudinal displacement of trajectory for spherical particle driven by an ambient forcing field pass multiple fixed obstacles, where θ is defined as slope angle and φ is defined as rotation angle. 9
- Figure 7. Mobility coefficient as a function of sphere-cylinder separation for the case of same particle and obstacle radius (Image reproduced from Nitsche²⁶) 14
- Figure 8. 3D point-particle model: a uniform ambient velocity field v with rotation angle φ and slope angle θ driving a freely suspended particle in Cartesian coordinate. 16
- Figure 9. Radial and tangential component velocity for touching collision when minimum surface separation is reached, where v_{xz} is the projection driving velocity v on x - z plane, v_t is the component velocity of v_{xz} in tangential direction and β_{xz} is the degree particle stays on the obstacle surface. 17
- Figure 10. Crossing and no crossing trajectories for two sizes of particles which have the same driving direction (Red trajectory: no crossing type trajectory; Blue trajectory: crossing type trajectory). 20
- Figure 11. Simulation setup of multiple cylinders where computational domain size is $30 \times 60 \times 30$ with Eulerian resolution $160 \times 320 \times 160$. Periodic boundary

conditions are applied in x and z direction.	23
Figure 12. Particle trajectories with a uniform force in x and y directions acting on it where $F_x=1$, $F_y=0.2$, $F_z=0$ for different b_{in} and $L_x=1.6 \pi$.	25
Figure 13. (a) The offsets of $F_x=1$, $F_y=0$, $F_z=0$ added on the particle passing single fixed obstacle with different b_{in} ; (b) The offsets of $F_x=1$, $F_y=0.2$, $F_z=0$ is adding on the particle passing single fixed obstacle with different b_{in} .	26
Figure 14. (a) Lateral displacement of three models ($a=R=0.2$). (b) Longitudinal displacement of three models ($a=R=0.2$)	28
Figure 15. (a) Migration angle as a function of forcing angle in 2D. (b) Transition angles as a function of slope angle and rotation angle. (c) Total displacement in y direction for $b_c=1.794\text{mm}$. (d) The displacement along y direction in each periodicity for $b_c=1.794\text{mm}$.	32
Figure 16. Periodicity of particle trajectory of experiment and Point-particle model for three sizes of particles at slope angle 32° .	35
Figure 17. Longitudinal displacement per post in z direction of different sizes of particles when slope angle is 20.5° (a) and 32° (c). Net longitudinal displacement per post in z direction of different sizes of particles when slope angle is 20.5° (b) and 32° (d).	37
Figure 18. (a)-(c) Theoretical transition angle from 2D case with particle trajectory type from 3D. (d) Comparison of longitudinal displacement per periodicity for different sizes of particles from simulation with point-particle model.	41
Figure 19. In-plane motion (a) and out-of-plane (b) motion for three different sizes of particles (1.5875mm, 2.38mm, 3.175mm) using point-particle model.	43

List of Tables

Table 1. Critical offset for three different sizes of particles from experiment results by calculating the transition angle.	34
Table 2. Critical offset for three different sizes of particles single particle-obstacle simulation.	39

1. Introduction

Microfluidics, a science of designing devices to manipulate and control volumes of fluid on the order of nanoliter scale, intersects subjects of engineering, chemistry, physics and biology. As an interdisciplinary field, the highly growing technology is used in biomedical, diagnostics, chemical analysis, and electronics industries¹ which is achieved by the development of lab-on-a-chip technology. A lab on a chip (LOC) is a device that integrates one or multiple laboratory functions on a single chip of only millimeter in length scale to a few square centimeters in size which is capable of handling and analyzing extremely small fluid volumes. LOC devices are often indicated as “Micro Total Analysis Systems” (μ TAS). Separation and continuous sorting of particles is one of the most important applications in microfluidic systems by using the characteristics of microscale flow which can be achieved fast and efficient and it can be applied in many areas, such as food industry, cell diagnostics, chemical analysis and so on. These separation techniques are classified as passive and active methods. For active methods, external fields are applied on separation, such as dielectrophoresis (DEP)², magnetic³, optical⁴ and acoustic⁵ methods. While for passive techniques, they use particle interactions, channel geometry and flow field instead of external fields to achieve particle separation which include pinched flow fractionation (PFF)⁶, microvortex manipulation (MVM)⁷, hydrodynamic filtration^{8,9} and micro-hydrocyclone⁸. Among these methods, deterministic lateral displacement (DLD) is a technique which can be implemented in both active and passive systems.

Deterministic lateral displacement is an emerging size-based separation technique in microfluidic which was first proposed by Huang⁹ as a passive method (Figure 1). Particles with size lower than the critical diameter will follow the streamlines and perform a ‘zigzag mode’ trajectory that the outlet of particles will be back to the original lane after passing through a tilted array of obstacles in laminar flow. Another ‘displacement mode’ trajectory is found when particle radius is larger than the critical diameter that particles will bump to its side lane after passing each row of obstacles. These obstacles can be in different shapes. DLD is also employed as an active separation technique when coupled with external fields (acoustic¹⁰, electric¹¹). Recent work demonstrates that DLD can also be available for the separation of deformable bodies and non-spherical particles^{12,13}.

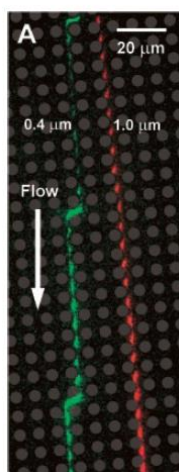


Figure 1. Image of micro-particles migrating in the first generation DLD by Huang showing two types of trajectories: zigzag mode for particle radius of $0.4 \mu\text{m}$ (green trajectory) and displacement mode for particle radius of $1.0 \mu\text{m}$ (red trajectory). Image reproduced from Huang et al⁹.

Different simulation methods have been used to study the separation of DLD system. A direct numerical simulation method (DNS) is used to simulate the motion of deformable particles through DLD and the relation between critical diameter and critical deformability

is studied. There exists a critical deformability that below which the critical diameter decreases as deformability increases¹⁴. Kulrattanarak et al. uses three-dimensional Lattice Boltzmann showing a mixed motion trajectory which is an irregular combination of zigzag and displacement mode¹⁵. Gaetano D'Avino performs 3D finite element method to simulate the motion of a spherical particle flowing through DLD ratchet and finds that the critical separation size has a dependence on the flow rate¹⁶.

In our group, in contrast to the flow-driven DLD, another modification DLD which uses an external constant force to drive the particle migrating in the system, is called force-driven DLD (f-DLD) systems. There is a kind named gravity-driven DLD (g-DLD) when gravity is applied as the driving force¹⁷⁻¹⁹. In the g-DLD, the suspended particles are driven through a periodic array of posts which is placed in a forcing angle of all range with gravity. They observe the presence of directional locking and demonstrate a high resolution for the separation of binary mixture of particles. They also perform a macroscale flow-driven DLD system by which an arbitrary forcing angle can be easily reconfigured.²⁰ In this system, a locked mode is observed at small forcing angle and they find that the transition from locked to zigzag mode occurs at larger forcing angle as particle size increases (see Figure 2). For both force-driven and flow driven DLD, the first transition angle or critical angle where particles bumping to another row of posts which results in a periodic zigzag trajectory from the bottom row in locked mode depends on the size of particles that critical angle increases as particle size increases^{18,21}. When the same constant driving force acts on particles of different size moving in a DLD system, they exhibit different periodic trajectories, which

leads to differences in migration direction, and they can be separated by size. Figure 2 shows the geometry of the DLD system with lattice space l . Two sizes of particles are driven by same forcing field passing through the lattice. The larger size particle is found to follow a locked mode trajectory and the smaller size particle is in a zigzag mode. There exists two angles, the forcing angle α and the migration angle β . For the smaller size of particle, the forcing angle α is an angle between driving field F and a column in the array (x axis), the migration angle is β line L with respect to x axis.

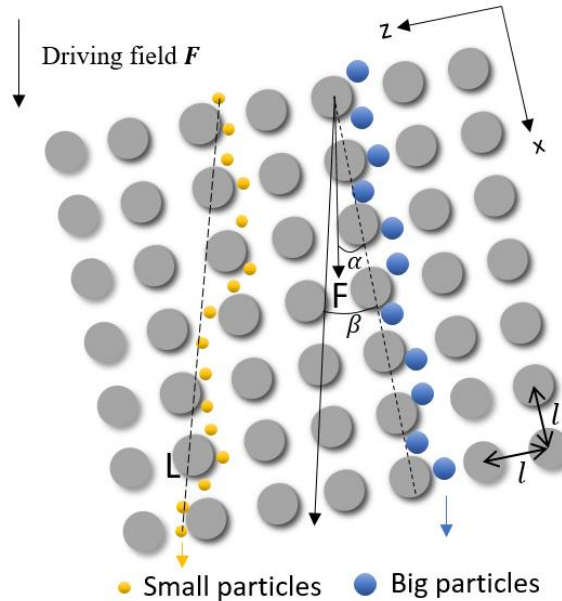


Figure 2. Schematic view of particle trajectories passing through a square periodic array of posts at two different forcing direction, where forcing angle α is an angle between driving field F and a column in the array (x axis), migration angle is β line L with respect to x axis.

In microfluidics, inertial forces are significant smaller than viscous force and the fluid flow is considered to be laminar flow with Reynolds number (Re) below 1. The Peclet number (Pe) is the ratio of convection rate and diffusion rate of particles and it is very high in microchannel²², ranging from 10 to 10^5 . Our group have also used different simulation

methods to study the mechanism of particle separation in DLD. Based on the fact of high Peclet number and small Reynolds number in DLD, we use Stokesian dynamics simulation of non-Brownian particles, which shows good agreement with experiment results²³. Molecular dynamics (MD) simulations are used on the motion of nanoparticles which enables to take Brownian motion, hydrodynamic interactions and roughness of the particles into account and shows the existence of directional locking²⁴. Based on the investigation from experiment and simulation (Figure 3), a 2D point-particle model is proposed to analyze the trajectory of suspended spherical particles moving through a square array of obstacles at zero Reynolds number in deterministic limit²⁵.

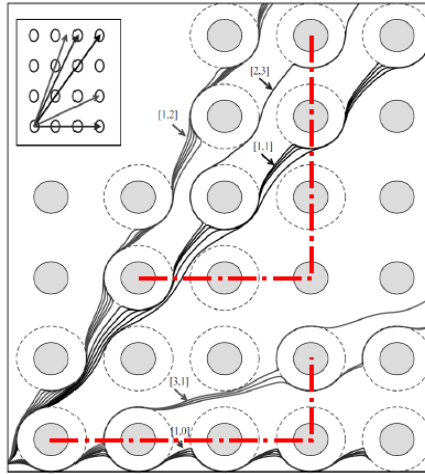


Figure 3. Particle trajectories showing directional locking with forcing direction ranging from 0 to 45°. Results are from Stokesian dynamics simulation and [1,0], [3,1], [1,1], [2,3] and [1,2] represents different periodicity of particle trajectories in locked mode.

We employ a simple point-particle model to describe two types of particle–obstacle collisions when a spherical particle moves pass a fixed cylindrical obstacle at zero Reynolds number. The model is under a dilute assumption that separation of posts is large enough so that the particle interacts with only one obstacle at a time. We work on Stokes

regime and we neglect fluid and particle inertia, as well as Brownian motion. There are two kinds of collisions which are from a simplification model to describe the trajectories causing by hydrodynamic and non-hydrodynamic forces. Firstly, the purely hydrodynamic collision results in a symmetric particle trajectory that the incoming and outgoing lateral displacements along the force direction perpendicular to the center line of obstacle are the same after collision (blue trajectory in Figure 4a). The other one, the touching collision, due to non-hydrodynamic interactions such as surface roughness, electrostatic repulsion, steric repulsion, etc., leads to a hard-wall potential which prevents the particle penetrate into a circular repulsive core with radius ε . Since all this type of trajectories have same minimum surface-to-surface separation between particle and obstacle, the outgoing trajectories coincide into one trajectory of which the outgoing offset is defined as critical offset b_c for all touching collisions (red and black trajectories in Figure 4a). Therefore, for hydrodynamic collisions, if $b_{in} > b_c$, then $b_{out} = b_{in}$ according to symmetry, for irreversible touching collisions, when $b_{in} \leq b_c$, then $b_{out} = b_c$ (Figure 4a). If only the net lateral displacement is considered, these two types of trajectories can be replaced with an equivalent model shown in Figure 4b, the point-particle model under the action of driving field F (a constant force or a flow field) driving a freely suspended particle in which obstacle radius R can be replaced by critical offset b_c and the spherical particle can be regarded as a point particle (Figure 4b). As shown, when $b_{in} > b_c$, the trajectory is fore-aft symmetric, we replace the physical trajectory with a straight line uninfluenced by the obstacle. For $b_{in} \leq b_c$, when this straight line intersects the new obstacle with radius

b_c , it will get a lateral displacement ($b_c - b_{in}$) and continue moving in a straight line at the tangent point of the obstacle.

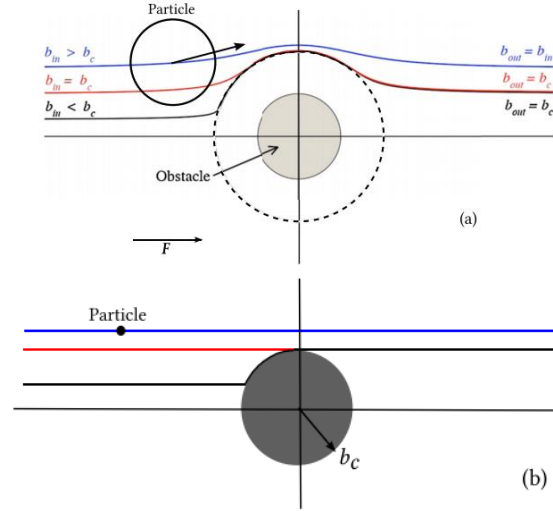


Figure 4. (a) Schematic view of two types of particle trajectories resulting from hydrodynamic collision (when $b_{in} > b_c$, then $b_{out} = b_{in}$) and non-hydrodynamic collision (when $b_{in} \leq b_c$, then $b_{out} = b_c$). (Reproduced from Balvin et al.²¹); (b) Point particle model of two dimensional case (Reproduced from Risbud and Drazer²⁵)

As particle moves through a square array of posts, if the forcing angle is above the first transition angle (α_c), which is also called the critical angle, the particle bumps to another column of obstacles, whereas the particle moves along the column of obstacles. In Figure 5, the particle comes out in an irreversible asymmetric trajectory with an outgoing offset b_c when the forcing angle exactly equals to the critical angle α_c . To obtain the theoretical critical offset, we use the simple geometry relation to express it as $b_c = l \sin \alpha_c$. So only when the forcing angle is larger than the critical angle α_c does the particle bump to another column of obstacle as [3,1] trajectory shown in Figure 3. Whereas the particle keeps in the same lane of obstacles show a periodicity as [1,0] in Figure 3.

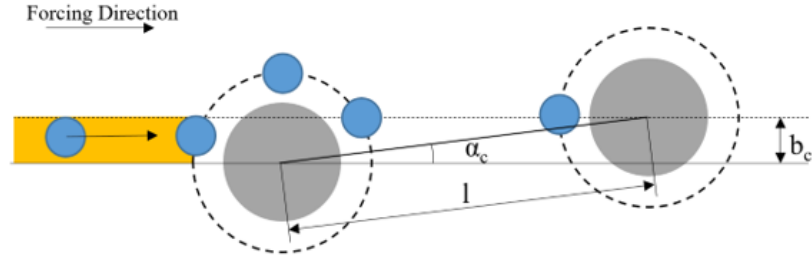


Figure 5. Schematic view of the forcing direction of particle exactly at the critical angle. In the second collision of particle with obstacle, the particle collides on the centerline of the obstacle, where critical offset b_c is the vertical distance between the centerlines of two obstacles.

In the 3D model we will discuss in this thesis, two new angles are introduced, slope angle θ and rotation angle φ to describe the driving field F . Since a new component force is added on the particle, the longitudinal displacement which is the displacement along the cylindrical obstacle needs to be taken into consideration. Figure 6 shows the lateral displacement and longitudinal displacement of a particle passing through 3D-DLD with a driving field of slope angle θ and rotation angle φ , where θ is the angle between driving direction and z axis, φ is the angle between the projection of driving direction on x - y plane with x axis. The lateral shift is the displacement of particle on the x - z plane and the longitudinal displacement is in the direction of y axis.

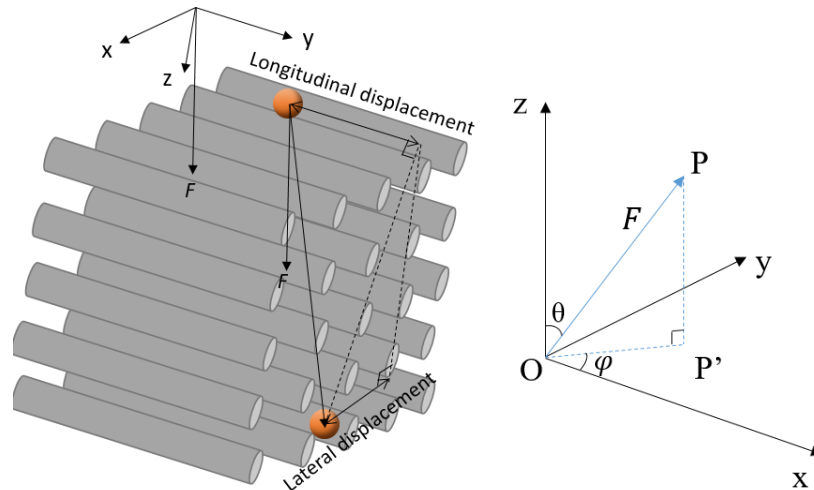


Figure 6. 3D-DLD on lateral displacement and longitudinal displacement of trajectory for spherical particle driven by an ambient forcing field pass multiple fixed obstacles, where θ is defined as slope angle and φ is defined as rotation angle.

All the previous works are done in 2D DLD system that are only focus on the lateral displacement of particles. In this thesis, we propose a 3D separation model by adding a constant force perpendicular to the cylindrical obstacle direction on the particles which will cause a longitudinal displacement to the particle. In 2D model, different size of particles can be separated by different migration directions at same forcing angle. However, some of the particles cannot be separated at one time since they have same migration directions so that they. For our 3D model, we take advantage of both lateral and longitudinal displacements simultaneously that separate particle of same lateral displacement by different longitudinal displacements. By applying both lateral longitudinal displacement, separation process can be more efficient. Given a certain forcing direction (slope angle and rotation angle), separation of multiple particles with different size can be achieved at only one process. Different models and simulation are studied in the thesis to help better understand the potential separation ability of this 3D system.

2. Numerical Method and Analytical Model

2.1 Objective

We study the motion of a suspended spherical particle driven by a constant force moving past single or multiple fixed cylindrical obstacles in a Stokes quiescent fluid. In previous work, the motion of particle is mainly focused on the plane which is perpendicular to the direction along cylinder. However, sometimes it is hard to separate the particles at one time only by in-plane motion since different size of particles may have same migration direction after moving through 2D-DLD. So, we propose the 3D-DLD model to study the out-of-plane motion of particle which is the motion along cylinders (longitudinal displacement). First, we compare the lateral displacement and longitudinal displacement of one particle moving past a single obstacle obtained using Nitsche's model (an approximate analytical solution to the mobility), the point-particle model and numerical simulations, focusing in the case of equal particle and obstacle radius. (Note that the analytical formulas given by Nitsche are only valid for such case.) Then, for multiple cylinders, we present a comparison of results obtained from point particle model and simulation with experimental results. Since in the simulations, the value of the critical offset of the particles results from the numerical implementation and cannot be controlled. As a result, we cannot make a direct comparison between the simulations and the experimental results. Therefore, we first compare the simulations to the point particle model and then we compare the point particle model to the experiments. Using these methods, we study the motion of particle passing

single obstacle and multiple obstacles case in three dimensional systems by both lateral and longitudinal displacements. This will give us guidance of the designation of the potential size-based particle separation system.

2.2 Nitsche's model²⁶

Nitsche considers a suspended spherical particle moving under the action of a uniform force around a fixed cylindrical fiber in a quiescent fluid. In Stokes flows, the velocity of the suspended particle U is linear in the constant driving force F , $U = M \cdot F$ where M is the mobility tensor determined by the geometry of particle and obstacle. Nitsche provides a set of empirical formulas to express the mobility as functions of particle-obstacle separation (r). Hyperbolic tangent is used as weighing functions between two parts: the far-field and lubrication regions.

At large separations, the far-field expressions of the mobility as functions of particle-fiber separation in radial $A(r)$, tangential $B(r)$ and axial $C(r)$ directions are proposed,

$$A(r) = \frac{1}{6\pi\mu a} \left(1 - \frac{117\pi}{128} \frac{a/r}{\ln(2/\varepsilon) + 1.7}\right) \quad (1)$$

$$B(r) = \frac{1}{6\pi\mu a} \left(1 - \frac{3\pi}{8} \frac{a/r}{\ln(2/\varepsilon) + 2.7}\right) \quad (2)$$

$$C(r) = \frac{1}{6\pi\mu a} \left(1 - \frac{63\pi}{128} \frac{a/r}{\ln(2/\varepsilon) + 2.2}\right) \quad (3)$$

where a is the radius of spherical solute, r is the center to center separation between particle and obstacle, μ is the viscosity of the fluid and ε the ratio of obstacle radius to particle-

obstacle distance.

For small gaps, lubrication theory yields the following functional forms for the leading order of mobility functions,

$$A(r) = \frac{1}{6\pi\mu a} \times 6\pi \left\{ \frac{3\pi}{\sqrt{2}} \left[\frac{3}{4}(r/R - 2) \right]^{-1} - \frac{151\pi}{60\sqrt{2}} \ln \left[\frac{3}{4}(r/R - 2) \right] + 19.4 \right\}^{-1} \quad (4)$$

$$B(r) = \frac{1}{6\pi\mu a} \times 6\pi \left\{ \frac{-\pi}{\sqrt{2}} \ln \left[\frac{3}{4}(r/R - 2) \right] + 19.5 \right\}^{-1} \quad (5)$$

$$C(r) = \frac{1}{6\pi\mu a} \times 6\pi \left\{ \frac{-20\pi}{7\sqrt{2}} \ln \left[\frac{3}{4}(r/R - 2) \right] + 20.09 + \frac{\left(\frac{12\pi}{7\sqrt{2}} \ln \left[\frac{3}{4}(r/R - 2) \right] + 4.65 \right)^2}{\frac{24\pi}{7\sqrt{2}} \ln \left[\frac{3}{4}(r/R - 2) \right] + 19.59} \right\}^{-1} \quad (6)$$

Figure 7 shows the mobility coefficient as functions of particle-obstacle separation when they are of same radius ($a/R=1$). Nitsche calculate the mobility coefficient when $r/R=3, 4, 5$ for the motion of spherical particle near a fixed finite-length cylinder. For the far-field region, the data points are $r/R=5, 10$ and there is a slightly discrepancy of the points at $r/R=5$. To quantitatively represent the dimensionless radial (m_r), tangential (m_t) and axial (m_a) mobility coefficients as functions of particle-obstacle separation, Nitsche uses the $\ln(r/R - a/R)$ as the independent variable to represent the dimensionless particle-obstacle separation and hyperbolic tangent to weigh the far- field (equation (1) - (3)) and the lubrication approximation equation ((4) - (6)). He gets the approximation mobility coefficient function as,

$$\begin{aligned}
m_{ii,approx} &= \frac{1}{2} \left(1 + \tanh\{a_{ii} \ln[(r/R - 1 - a/R)/b_{ii}]\} \right) (\text{far field}) \\
&+ \frac{1}{2} \left(1 - \tanh\{a_{ii} \ln[(r/R - 1 - a/R)/b_{ii}]\} \right) (\text{lubrication}) \\
&- c_{ii} / \cosh\{a_{ii} \ln[(r/R - 1 - a/R)/b_{ii}]\}
\end{aligned} \tag{7}$$

,where a_{ii} determines the distance that above which far field to lubrication formulas occur, b_{ii} is the dimensionless surface-to-surface separation between particle and obstacle where both far field and lubrication formulas coincide, and c_{ii} is a number to fit the formula with numerical calculations (see Figure 7). Then, the mobility functions are then written as,

$$\begin{aligned}
A(r) &= \frac{1}{6\pi\mu a} \left\{ \frac{1}{2} \left(1 + \tanh\{2 \ln[(r/R - 2)/1.57]\} \right) \left(1 - \frac{a}{r} \frac{117\pi}{128} \frac{1}{\ln(2r/R) + 1.7} \right) \right. \\
&+ \frac{1}{2} \left(1 - \tanh\{2 \ln[(r/R - 2)/1.57]\} \right) \times 6\pi \left\{ \frac{3\pi}{\sqrt{2}} \left[\frac{3}{4} (r/R - 2) \right]^{-1} - \frac{151\pi}{60\sqrt{2}} \ln \left[\frac{3}{4} (r/R - 2) \right] + 19.4 \right\}^{-1} \\
&\left. - 0.09 / \cosh\{2 \ln[(r/R - 2)/1.57]\} \right\}
\end{aligned} \tag{8}$$

$$\begin{aligned}
B(r) &= \frac{1}{6\pi\mu a} \left\{ \frac{1}{2} \left(1 + \tanh\{2 \ln[(r/R - 2)/1.034]\} \right) \left(1 - \frac{a}{r} \frac{3\pi}{8} \frac{1}{\ln(2r/R) + 2.7} \right) \right. \\
&+ \frac{1}{2} \left(1 - \tanh\{2 \ln[(r/R - 2)/1.034]\} \right) \times 6\pi \left\{ \frac{-\pi}{\sqrt{2}} \ln \left[\frac{3}{4} (r/R - 2) \right] + 19.5 \right\}^{-1} \\
&\left. - 0.06 / \cosh\{2 \ln[(r/R - 2)/1.034]\} \right\}
\end{aligned} \tag{9}$$

$$\begin{aligned}
C(r) &= \frac{1}{6\pi\mu a} \left\{ \frac{1}{2} \left(1 + \tanh\{2 \ln[(r/R - 2)/1.31]\} \right) \left(1 - \frac{a}{r} \frac{63\pi}{128} \frac{1}{\ln(2r/R) + 2.2} \right) \right. \\
&+ \frac{1}{2} \left(1 - \tanh\{2 \ln[(r/R - 2)/1.31]\} \right) \times 6\pi \left\{ \frac{-20\pi}{7\sqrt{2}} \ln \left[\frac{3}{4} (r/R - 2) \right] + 20.09 \right. \\
&\left. \left. + \frac{\left(\frac{12\pi}{7\sqrt{2}} \ln \left[\frac{3}{4} (r/R - 2) \right] + 4.65 \right)^2}{\frac{24\pi}{7\sqrt{2}} \ln \left[\frac{3}{4} (r/R - 2) \right] + 19.59} \right\}^{-1} \right. \\
&\left. - 0.07 / \cosh\{2 \ln[(r/R - 2)/1.31]\} \right\}
\end{aligned} \tag{10}$$

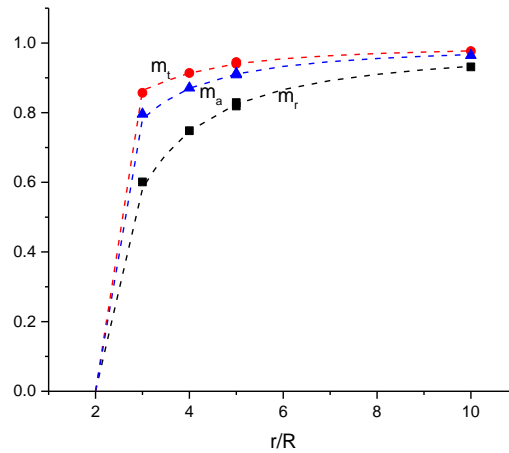


Figure 7. Mobility coefficient as a function of sphere-cylinder separation for the case of same particle and obstacle radius (Image reproduced from Nitsche²⁶)

From the equations, we can see that the mobility functions in all three directions are only dependent on the particle-obstacle separation r . The mobility functions $A(r)$ and $B(r)$, determine the particle motion in the plane perpendicular to the obstacles. They also determine the particle-obstacle separation since the separation is measured in this plane. The mobility function $C(r)$ only affects the motion of the particle in the direction along the cylinders. Therefore, if $A(r)$ and $B(r)$ are fixed, a different value in $C(r)$ only causes a difference in longitudinal displacements and all the projection of trajectories on the plane will coincide with each other. The in-plane motion is independent with the out-of-plane motion. Thus, we can divide the analysis of the particle trajectory into two parts: one is the projection of the trajectory onto the plane perpendicular to the obstacles which is determined by the radial and tangential mobility functions, the other one is the displacement in the direction along the obstacles which is determined by axial mobility function after we get the separation using in-plane motion mobility functions.

2.3 Point-particle model

2.3.1 Single obstacle

In the introduction part, we present the 2D point-particle model proposed by our group. Based on the 2D case, we extend this model to a three dimensional analysis that the field driving the particle is an arbitrary angle with velocity on the particle expressed as $\mathbf{v} = v_x \mathbf{e}_x + v_y \mathbf{e}_y + v_z \mathbf{e}_z$ instead of a driving force F in the 2D model. We make the same assumptions that fluid and particle inertia are neglected (small Reynolds number and Stokes number). Also, we assume infinitely large Peclet number (non-Brownian motion).

For hydrodynamic interactions, the particle point moves in the direction of the driving velocity field acting on it, while for the touching collisions, when the point particle reaches the minimum surface separation ε , the motion of the particle in the longitudinal direction is not simply following the driving velocity. In order to get this longitudinal displacement at collision period, a new calculation method is proposed, in which the time of particle moving on the surface of obstacle is evaluated in the point particle model. When the particle collides with the obstacle surface, the component velocity in the radial direction vanishes and the tangential component velocity drives the particle to go around the surface of the obstacle and the particle leaves the obstacle when it gets to the tangent point. Here, we assume that the velocity in y direction which is the direction along the cylinder to be constant all the time since we want to use this 3D model to predict the trend of longitudinal

displacement with driving angles and the exact axial velocity is not available and cannot be calculated analytically. When no collision happens, the particle migrates in the direction of the driving velocity.

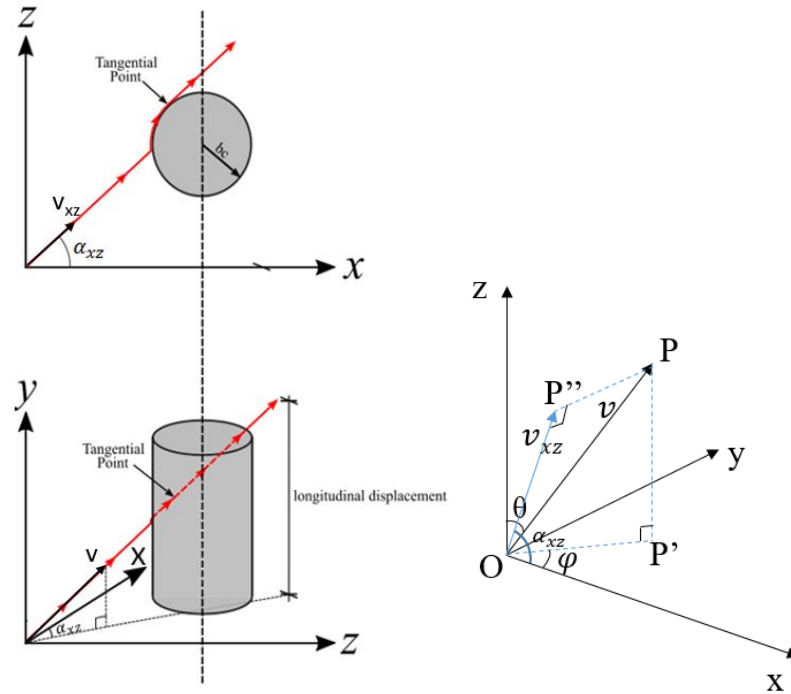


Figure 8. 3D point-particle model: a uniform ambient velocity field v with rotation angle φ and slope angle θ driving a freely suspended particle in Cartesian coordinate.

We use two angles to describe the velocity field (or driving force) pointed in space, the slope angle θ is an angle between velocity v (OP) and z axis, the rotation angle φ is the angle between projection of v on x - y plane (OP') and x axis (Figure 8). The velocity v can be divided into two components, one of which is the projection velocity on the x - z plane v_{xz} (OP'') that it drives particles to move in the 2D plane, another of which is component velocity v_y ($P'P$) driving particles along the posts. α_{xz} is an angle between v_{xz} and x axis in x - z plane which is the in-plane driving force.

We analyze these two component velocities to establish the 3D point-particle model.

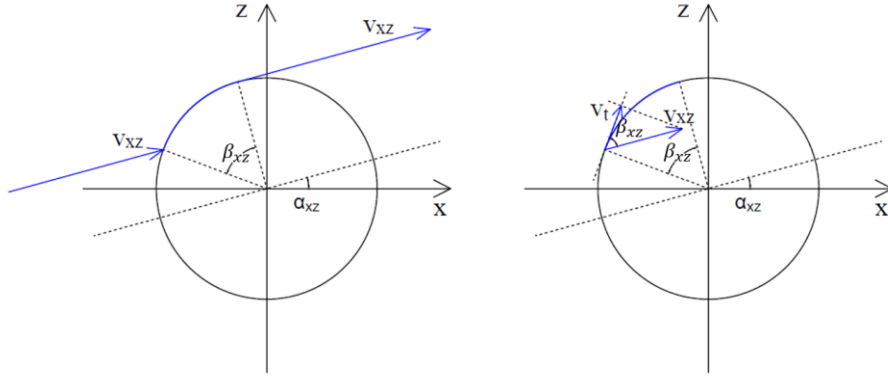


Figure 9. Radial and tangential component velocity for touching collision when minimum surface separation is reached, where v_{xz} is the projection driving velocity v on x - z plane, v_t is the component velocity of v_{xz} in tangential direction and β_{xz} is the degree particle stays on the obstacle surface.

We then present the way to calculate the displacement in y for touching collision when minimum surface separation is reached. To calculate the total time of particle moving on the surface of obstacle, angular velocity is expressed using a projection velocity on the x - z plane v_{xz} .

$$\frac{d\beta_{xz}}{dt} = \omega = \frac{v_t}{b_c} = \frac{v_{xz} \cos \beta}{b_c} \quad (11)$$

Integrating on both sides to get time t ,

$$\int \frac{d\beta_{xz}}{\cos \beta_{xz}} = \int \frac{v_{xz}}{b_c} dt$$

$$t = -\frac{b_c}{v_{xz}} \ln(\sec(-\beta_{xz}) + \tan(-\beta_{xz}))$$

Then we make an assumption that the velocity in the y direction will always be a constant velocity v_y for both types of collisions. The longitudinal displacement for touching collision when minimum surface separation is reached is,

$$\Delta y = -\frac{v_y b_c}{v_{xz}} \ln(\sec(-\beta_{xz}) + \tan(-\beta_{xz})) \quad (12)$$

where Δy is the displacement in y direction, v_t is the tangential velocity, b_c is the critical offset related with particle and obstacle radius, β_{xz} is the angle which starts from the touching point and ends in the leaving point of the particle on the surface (Figure 9).

Here, the velocity along obstacle direction is assumed to be constant. However, from Nitsche's model we know that the velocity in y direction decreases when particle gets closer to the obstacle and increases when it leaves. The limitation of Nitsche's model is that it is only valid for the case of equal radii of particle and obstacle. The simple assumption we make in the point-particle model helps us predict the longitudinal displacement and will not affect the particle motion in the x-z plane. Also, since the motion on the obstacle surface in y direction is calculated by the integral of total time, the trajectory in this case is not the exact one but an averaged motion. This will not influence our results discussion on longitudinal displacement. Based on this 3D point-particle model, when critical offset b_c , rotation angle φ and slope angle θ are given, we can get the particle trajectory and calculate its lateral and longitudinal displacement.

2.3.2 Multiple obstacles

We assume a "dilute limit" that single particle only interacts with one obstacle in a collision as the space between obstacles are sufficiently large. Under this assumption, also the exact trajectory at collision is ignored since we discussed in previous part that this will

not affect the value of displacement in y direction. If only the incoming, outgoing offsets and longitudinal displacement are studied, the particle trajectory can be replaced by a point particle moving in a straight line past an obstacle with an effective radius, the critical offset b_c . The particle is driven at an arbitrary angle into space related with slope angle and rotation angle mentioned above. The touching collisions lead to both lateral displacement and longitudinal displacement compared with the driving direction displacement after passing multiple obstacles.

In the multiple obstacles system, all cylinders are set along y direction with radius R to be 1 and lattice space l between two cylinders to be 6. The system contains 200 obstacles of which 20 in z direction and 10 in x direction (Figure 10). The sizes of the particles we study are 1.5875mm, 2.37mm and 3.175mm in diameter which are the same as those in the experiment. The initial point of particle is at $(l - b_c, 0, l - b_c)$ to ensure that the particle will have collision with the first obstacle. In this multiple obstacles system, the value of b_c are chosen from experiment data by measuring the transition angles of different sizes of particles, so that other results from the point-particle model can be compared with experiment results. If b_c is known, we can get the trajectory of the particle passing multiple cylinders at any driven direction using point-particle model. So we use slope angle ranging from 0 to 45° and rotation angle ranging from 0 to 90° with a given b_c to get the trajectory of particle at a certain forcing direction.

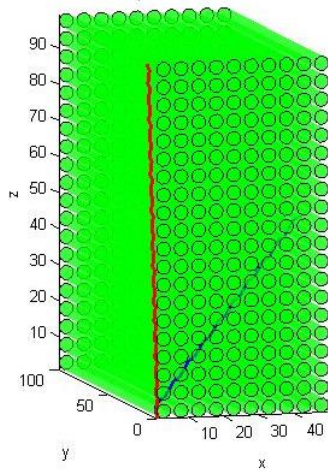


Figure 10. Crossing and no crossing trajectories for two sizes of particles which have the same driving direction (Red trajectory: no crossing type trajectory; Blue trajectory: crossing type trajectory).

2.4 Simulation method

In this part, we consider three dimensional simulation of a suspended particle driven by a constant force moving pass one or multiple cylinders in quiescent fluid at zero Reynolds number that inertia is neglected. The code we use is from Prof. Bagchi's group and in the following part is a brief introduction of the code.

The governing equations of this flow solver are

$$\begin{aligned} \frac{\partial \mathbf{u}}{\partial t} + \mathbf{u} \cdot \nabla \mathbf{u} &= -\nabla p + \frac{1}{\text{Re}} \nabla^2 \mathbf{u} + \mathbf{f} \\ \nabla \cdot \mathbf{u} &= 0 \end{aligned} \quad (13)$$

In the time-integration, the discrete form is as below where the viscous terms use the Crank-Nicolson scheme and the nonlinear terms are treated explicitly using a second-order Adams-Bashforth scheme,

$$\frac{\mathbf{u}^{n+1} - \mathbf{u}^n}{\Delta t} = -\frac{3}{2}(\mathbf{u} \cdot \nabla \mathbf{u})^n + \frac{1}{2}(\mathbf{u} \cdot \nabla \mathbf{u})^{n-1} + \nabla p^{n+1} + \frac{1}{\text{Re}} \cdot \frac{1}{2}(\nabla^2 \mathbf{u}^{n+1} + \nabla^2 \mathbf{u}^n) + \mathbf{f} \quad (14)$$

We then apply projection method:

$$\frac{\mathbf{u}^* - \mathbf{u}^n}{\Delta t} = -\frac{3}{2}(\mathbf{u} \cdot \nabla \mathbf{u})^n + \frac{1}{2}(\mathbf{u} \cdot \nabla \mathbf{u})^{n-1} + \frac{1}{\text{Re}} \cdot \frac{1}{2}(\nabla^2 \mathbf{u}^* + \nabla^2 \mathbf{u}^n) + \mathbf{f}$$

$$\frac{\mathbf{u}^{n+1} - \mathbf{u}^*}{\Delta t} = -\nabla p^{n+1} \quad (15)$$

Where \mathbf{u}^* is the predicted velocity at an intermediate time level between n and $n+1$, Δt is the time step size. The next step involves solving a Poisson equation for the pressure as,

$$\nabla^2 p^{n+1} = \frac{1}{\Delta t} \nabla \cdot \mathbf{u}^* \quad (16)$$

The velocity obtained from the prediction step is then projected onto a divergence-free space to obtain the velocity at time level $n+1$ as,

$$\mathbf{u}^{n+1} = \mathbf{u}^* - \Delta t \nabla p^{n+1} \quad (17)$$

In order to get the trajectory of the particles in the flow field, leapfrog integration is used by calculating the total torques and forces acting on the particle from fluid.

To simulate the non-hydrodynamic interaction, a repulsive force is applied on the surface of the particle. When the surface-to surface separation of particle and obstacle is smaller than two grids length, the repulsive force is inversely proportional to cubic of the separation, while at larger separation no repulsive force is added on the particle.

2.4.1 Single obstacle

The resolution used in single obstacle simulation is $320 \times 80 \times 320$ with domain size $8\pi \times 2\pi \times 8\pi$ and dimensionless timestep in the simulation is 0.001. The domain is

bounded by two infinite flat walls parallel with x-z plane and no-slip conditions are applied at the top and bottom of walls. Periodicity boundary conditions are used in x and z directions to reduce the size of computational domain. The uniform force F adding on the particle is dependent with rotation angle φ and slope angle θ as $(F \cos \theta \cos \varphi, F \cos \theta \sin \varphi, F \sin \theta)$. And all the simulations are at zero Reynold number limit and all the parameters are dimensionless.

2.4.2 Multiple obstacles

To study the motion of a suspended particle moving in the three-dimensional DLD system, multiple obstacles along y direction are put in the computational domain as in Figure 11. All the simulations are run in the limit of zero Reynolds and timestep is set to be 0.001. In the code, periodic boundary conditions are applied in x and z directions as they are infinite long and no-slip boundary conditions are used in the top and bottom of walls perpendicular to y direction. The computational domain size is $30 \times 60 \times 30$ with Eulerian resolution $160 \times 320 \times 160$. The size of obstacle and particles are the same with the what we use in point-particle model and experiment. The lattice space between obstacles are 6 and we assume a dilute limit that the particle only interacts with single obstacle in one collision.

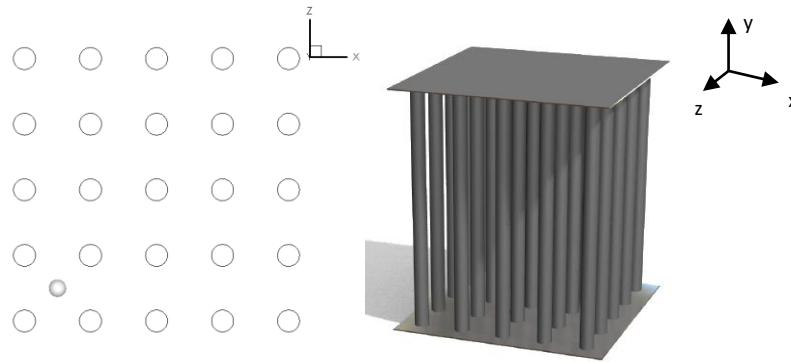


Figure 11. Simulation setup of multiple cylinders where computational domain size is $30 \times 60 \times 30$ with Eulerian resolution $160 \times 320 \times 160$. Periodic boundary conditions are applied in x and z direction.

Since the existence of walls at top and bottom of the simulation box, we find the velocity in y direction decreases when the particle gets very close to the wall. To reduce such influence, we only collect data in a certain region in the y direction (from 12 to 48). Also, we set L_x and L_z to be 30 which is a more effective length to reduce periodicity boundary effects because of the motion of particle both in x and z directions.

3. Results and discussions for single obstacle

3.1 Forcing direction angles from 2D to 3D

In the two-dimensional model, the forcing angle of particle is only in the x-z plane since particle migrates on this plane. While in the 3D system, this forcing angle is dependent with rotation angle φ and slope angle θ mentioned above. In order to make the motion of particle in 3D comparable with 2D case, a projection angle on the x-z plane (α_{xz} : in-plane forcing direction) of the forcing direction is proposed (Figure 8) and the relation of α_{xz} with rotation angle θ and slope angle can be expressed as,

$$\alpha_{xz} = \arctan(\tan\theta\cos\varphi) \quad (18)$$

Then, we regard the motion of particle in 3D as two separate motions, one of which is the motion in x-z plane that causes a lateral shift and the other is out-of-plane motion that a longitudinal displacement is obtained. In the following results discussion, we compare this in-plane forcing direction α_{xz} with 2D forcing angle to see the relation between 2D and 3D model.

3.2 Results from different models for single obstacle

3.2.1 Nitsche's model

Mobility functions (8) - (10) are used to calculate the trajectory of particle driven by a constant force ($F_x=1$, $F_y=0.2$, $F_z=0$) for different incoming offsets (see Figure 12). Since these functions are only in the case of same radius of particle and obstacle, we set $a=R=0.2$.

We show that the incoming and outgoing offsets (b_{in} and b_{out}) are almost the same using Nitsche's model and the projection trajectories on x-z plane are nearly symmetric. For each trajectory in Figure 12, particle starts at $(-0.8 \pi, b_{in})$ and ends at $(0.8 \pi, b_{out})$. By defining different b_{in} , we can get the position of particle at every timestep and b_{out} using Nitsche's mobility functions.

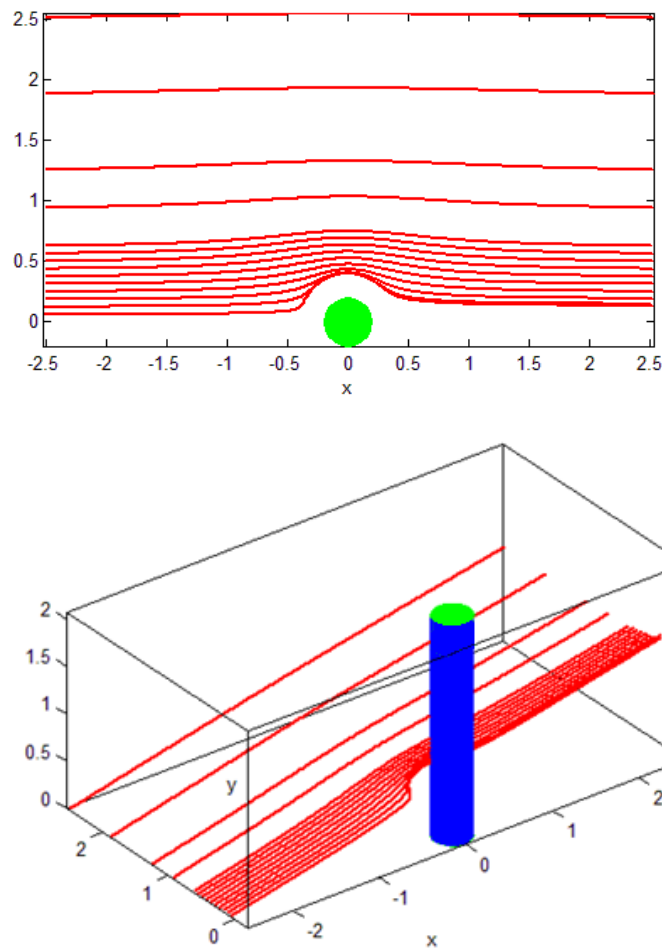


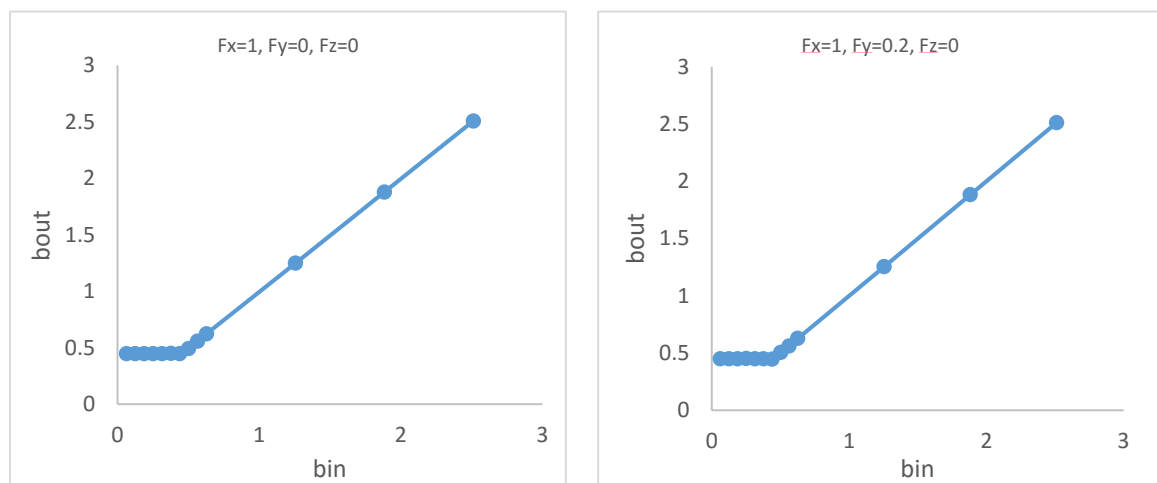
Figure 12. Particle trajectories with a uniform force in x and y directions acting on it where $F_x=1$, $F_y=0.2$, $F_z=0$ for different b_{in} and $L_x=1.6 \pi$.

Figure 12 shows the particle trajectory for different b_{in} , in Nitsche's model only hydrodynamic interaction is considered which gives us symmetric projection trajectories

in Stoke regime. There is some trajectories when b_{in} is small showing asymmetric. This is caused by numerical error that when we set a smaller timestep size, the trajectories near the obstacle will get better resolution. And for large b_{in} , the particle trajectory is almost a straight line migrating in the driving direction that we may consider for large separation the interaction between particle and obstacle is very little and this interaction increases as they come closer.

3.2.2 Simulation

We simulate the particle trajectories moving through a fixed cylinder when a uniform force acting on it in quiescent fluid at zero Reynold number. We find in Figure 13 that b_c (lateral critical offset) keeps constant when force in y varies. The axial forces cause differences in longitudinal displacement but will not have an influence on the lateral displacement.



Critical offset b_c for $F_x=1$, $F_y=0.2$, $F_z=0$ is from the projection trajectory on the x-z plane, also we find that these projection trajectories coincide with the trajectories for the case of $F_x=1$, $F_y=0$, $F_z=0$ that we can relate the 3D model of b_c with the 2D model by simulating the one particle-obstacle case to get the b_c first and then using $b_c = l \sin \theta_c$ to predict the transition angle of the 3D-DLD system as 2D. In the simulation, a repulsive force is applied on the particle to simulate the non-hydrodynamic interaction when particle gets very close to the obstacle which results in a hard-wall potential so that we get to the critical offset b_c . However, the non-hydrodynamic interaction is due to surface roughness, electrostatic repulsion, steric repulsion and so on that we cannot easily accomplished by simulation. Because of this limitation, we cannot get the same critical offset as what we get from experiment. Then we don't compare the simulation with the experiment results but only compare it to the point-particle model.

3.2.3 Comparison of three models

We then make a comparison of these three models on the lateral displacement and longitudinal displacement for single obstacle of the same size with particle ($a=R=0.2$) that in the simulation and Nistche's model the driving force is set as $F_x=1$, $F_y=0.2$, $F_z=0$ and in the point-particle model the velocity ratio v_x/v_y is set to to be 5 and $v_z=0$, the effective radius b_c to be 0.445 same with critical offset from simulation which makes these models to be comparable.

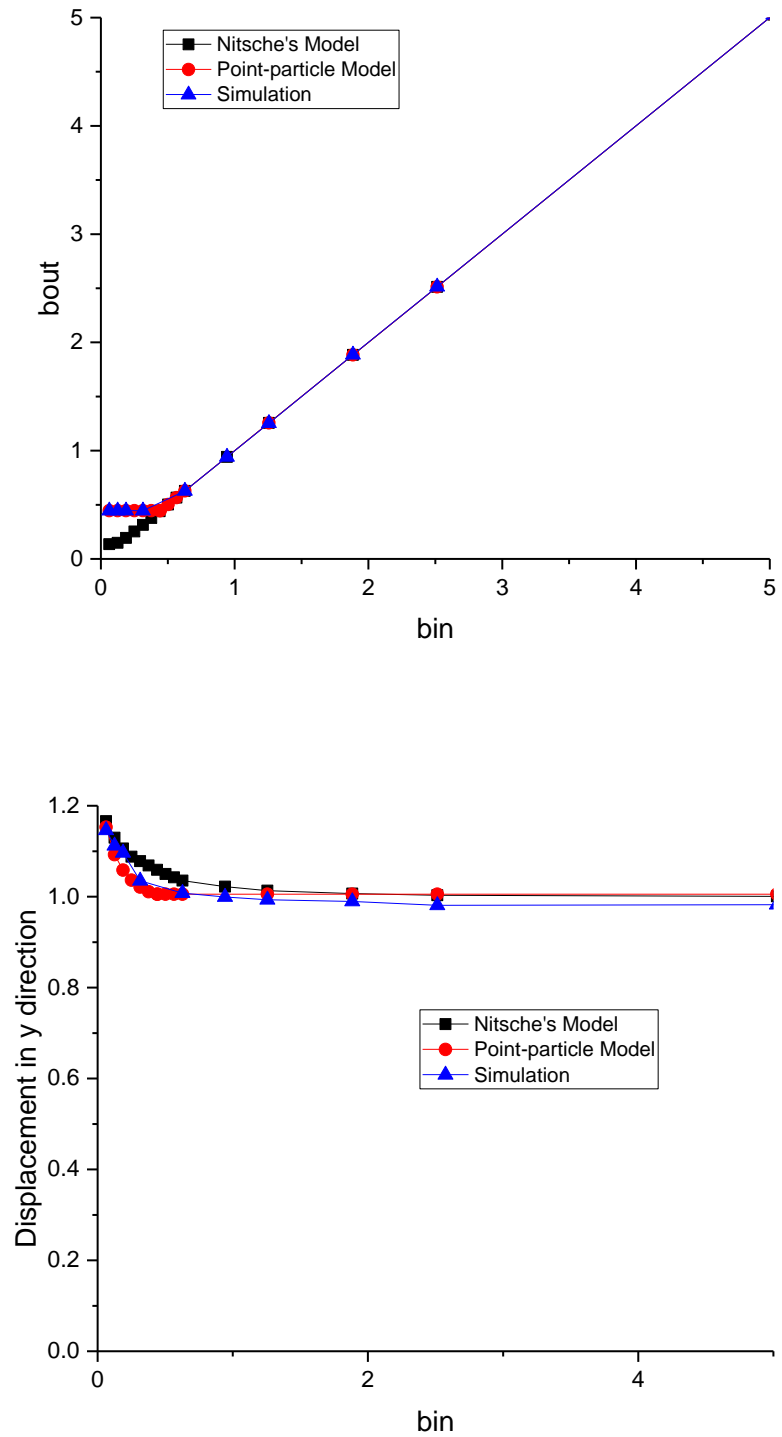


Figure 14. (a) Lateral displacement of three models ($a=R=0.2$). (b) Longitudinal displacement of three models ($a=R=0.2$)

From the plots, we see that with large b_{in} , the displacement in y approximately equals to 0.32π which is the value that the particle migrates only in the direction of the driving force in no obstacle case. So we can regard that the interaction with obstacle influences little on the particle trajectory for large b_{in} and we assume that the particle moves along forcing direction in such case. As b_{in} becomes smaller, the longitudinal displacement increases, the influence by the obstacle becomes larger and it gets to the maximum value when the incoming of particle is close to the center line the obstacle. It is reasonable for the assumption of our point particle model in the longitudinal displacement that collision will lead to an increase on the displacement along obstacles and at large separation the migration direction is consistent with driving direction.

4. Results in an array

4.1 Results, transition, displacement in y (Point-particle model)

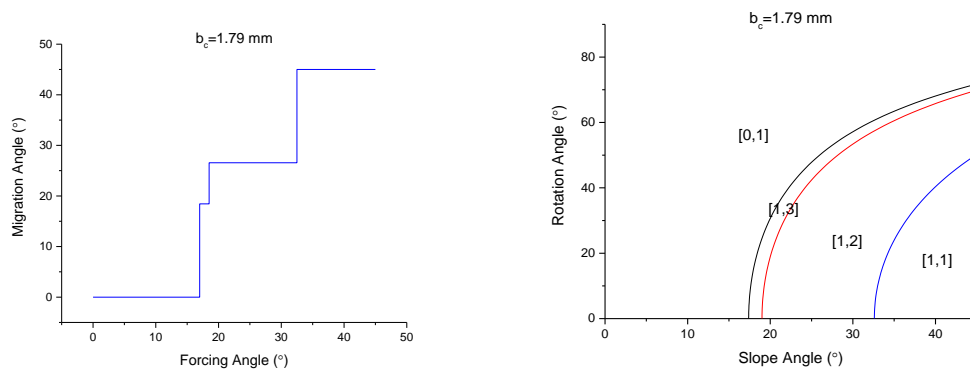
In 2D case, the theoretical critical angle α_c can be calculated by using equation $b_c = l \sin \alpha_c$ when critical offset and lattice space are given. For the 3D model, this critical angle is an angle in the x-z plane which can be expressed by rotation angle and slope angle. We want to see if this critical angle still works for the 3D case. The transition of crossing can be seen at this critical angle which means that the added force in y direction do not have an influence on the periodicity and migration angle of the particle projected trajectory on the x-z plane. In this part, we use point particle model to analyze the trajectory of particle passing a square array of obstacles and we assume the critical offset equals to the sum of particle and obstacle radius ($b_c = a + R$). First, we calculate the theoretical first transition angle or critical angle using equation 18 by rotation angle and slope angle (Figure 15a). Then we plot different trajectories type (crossing and no crossing) for different angles to see where transition occurs (Figure 15b-d). By no crossing type of trajectory, we mean that the particle will only go along one column of obstacles in z direction. And crossing type is that the particle will bump to other columns in x direction as it moves in z direction.

The critical angles in the figures in black solid lines are calculated using the equation 18 where α_{xz} equals to the critical angle got from $\alpha_c = \arcsin(b_c/l)$ in 2D system and we show an excellent fit that the transition angle from crossing to no crossing of 3D model has same value in the 2D case. The velocity added on the particle in the y direction will only

cause a longitudinal displacement and we can use the same equation to predict when there will be a transition in 3D system.

Using point particle model, the displacement in y direction with different periodicities are studied. We use $[p,q]$ to represent the periodic trajectory as the 2D case that successive collisions occur when particle moves p lattice units in x direction and q lattice units in z direction. The periodicity of $[0, 1]$ means that the particle will always move in the z direction (no crossing) and for this periodicity there will be the most number of collision times with the obstacles (20 times for our model).

We can get the staircase plot of migration angle versus forcing angle and using rotation angle and slope angle in 3D case to represent the transition angle where periodicity changes. The trajectories got from the point particle model fit these curves and longitudinal displacements are studied when one collision occurs, as well as the longitudinal displacements after particle moving through 20×10 obstacles.



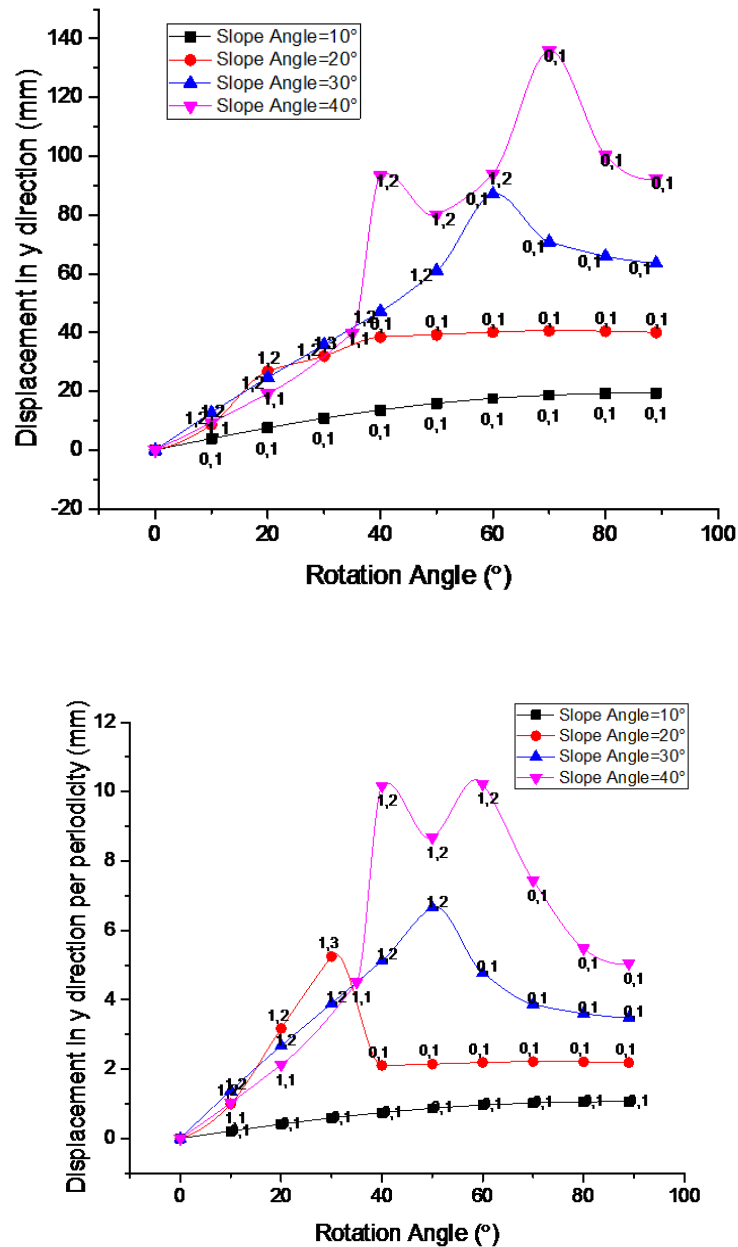


Figure 15. (a) Migration angle as a function of forcing angle in 2D. (b) Transition angles as a function of slope angle and rotation angle. (c) Total displacement in y direction for $b_c=1.794\text{mm}$. (d) The displacement along y direction in each periodicity for $b_c=1.794\text{mm}$.

Here, we find that at same slope angle the displacement near transition angle is larger than other rotation angles for the same periodicity. Since at transition angle, the particle

stays a longer time on the surface of the obstacle and keeps a uniform velocity in y direction which results in the axial displacement larger than the no collision ones or other angles. Also, for the same size of particle increasing slope angle leads to a larger longitudinal displacement. This difference in longitudinal displacement gives us the possibility to separate particles not only in the locking mode of migration angle, but we can also take the longitudinal displacement into consideration.

4.2 Comparison of point particle model with experiments

We compare the experimental data with the point particle model keeping b_c for each size of the particle consistent. If there are no collisions occur in the system which means the particle moves in the direction of the driving force, then the displacement in y increases as rotation angle becomes larger under certain slope angle. Collisions with obstacle will result in an increase in the displacement in y direction. Although this longitudinal displacement change is small for each collision, periodic collisions make every longitudinal displacement to accumulate and lead to a big difference in the displacement along obstacles compared with no collision cases. So the no crossing type trajectory near critical angle gets the maximum longitudinal displacement since it collides with every post in z direction and for duration time of each collision is the longest.

We get the particle trajectory using point-particle model by defining critical offset b_c obtained from experiment (Table 1) and in Figure 16 we show the periodicity of particle

trajectory by counting the number of posts the particle cross in x direction (p) and z direction (q) during one period of the trajectory. We then plot the displacement along y direction per periodicity. We also present an averaged longitudinal displacement to represent the value when particle moving pass one obstacle in z direction by using longitudinal displacement per periodicity divided by q and compare these results to experiment. And the in-plane forcing angle is calculated by equation 18 using rotation angles and slope angle. By applying this angle, we can relate the 3D model with 2D case.

Particle Size D (mm)	Critical Offset b_c (mm)	Theoretical Critical Angle α_c ($^\circ$)
1.5875	0.57	5.45
2.38	1.14	10.95
3.175	1.49	14.38

Table 1. Critical offset for three different sizes of particles from experiment results by calculating the transition angle.

Coupled with critical offset from experiment, we apply point-particle model by using different rotation angles ranging from 20° to 80° and a slope angle of 32° . Since we didn't track the periodicity of slope angle at 20.5° in the experiment, so we just plot the periodicity comparison between our model and experiment for slope angle of 32° . From the plot, we see that for larger size of particles, the periodicity (p/q) fit better. This is because that for smaller size of particle, the periodicity type is more complex making it more difficult to track and in the experiment the particle trajectory is an averaged motion.

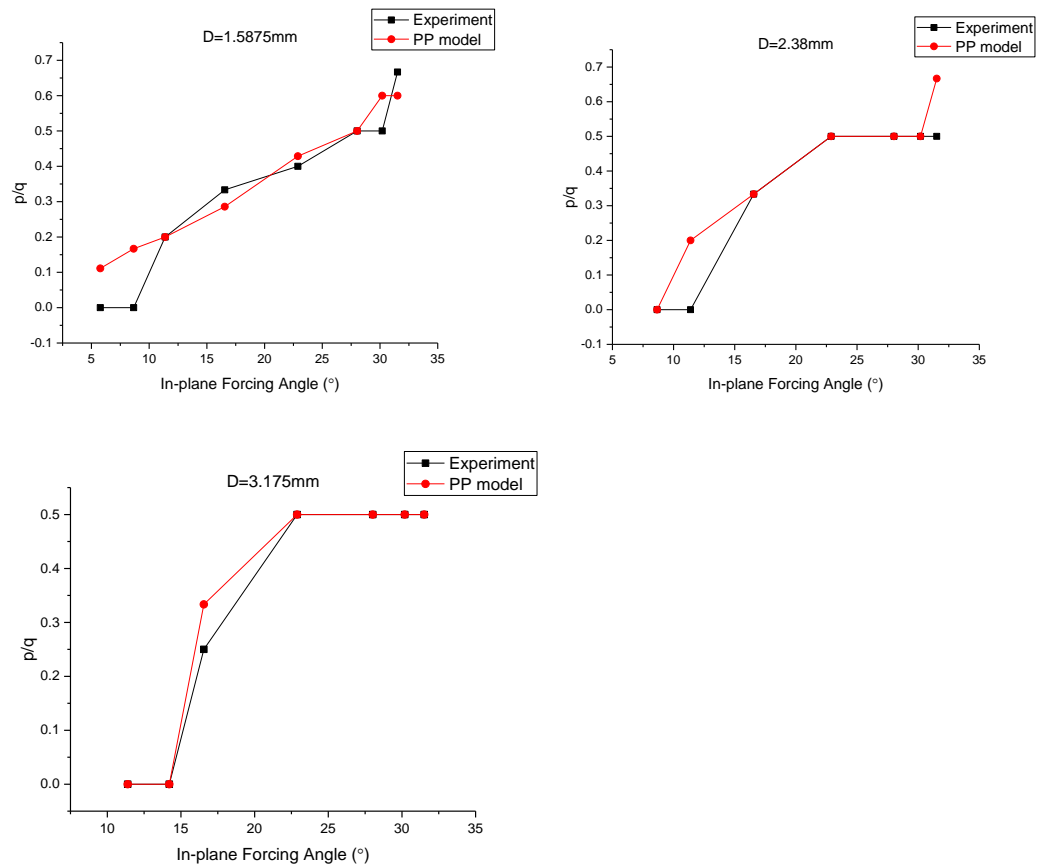
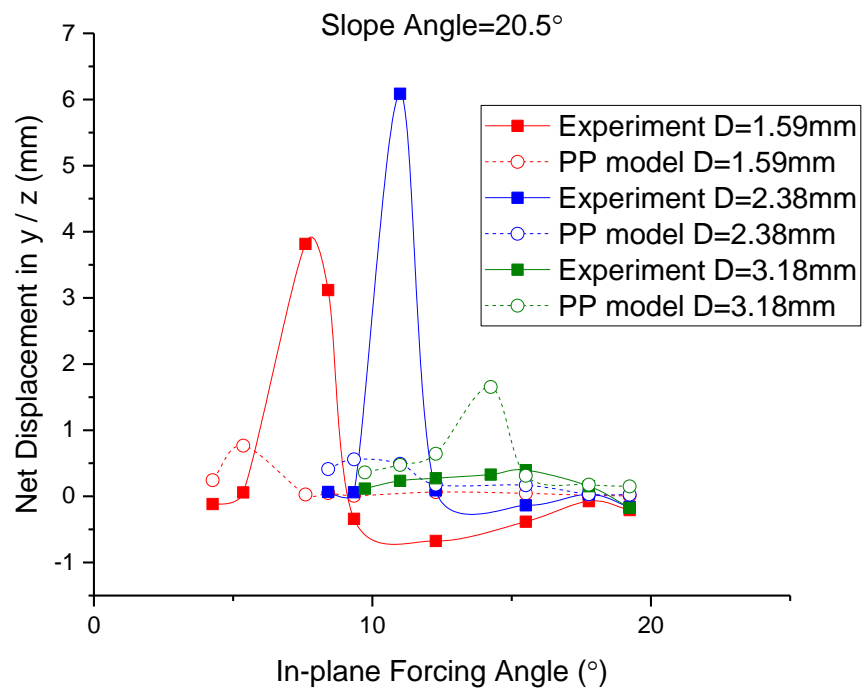
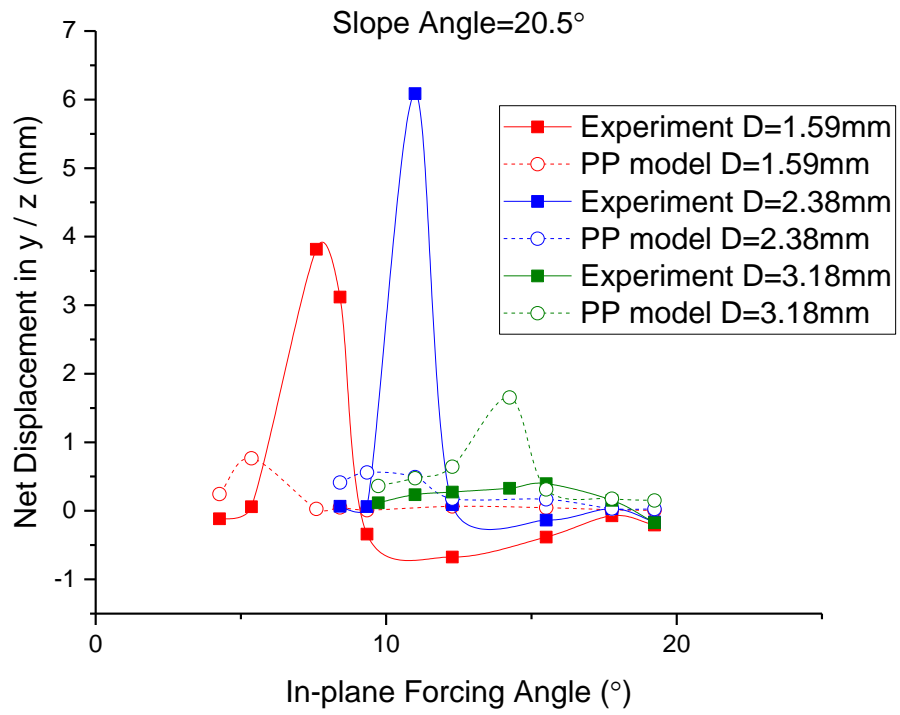


Figure 16. Periodicity of particle trajectory of experiment and Point-particle model for three sizes of particles at slope angle 32° .

In Figure 16, We compare the displacement in y direction using two different slope angles 20.5° and 32° with rotation angles ranging from 20° to 80° for each periodicity and the net displacement is calculated by subtract the displacement y direction when no collision occurs.



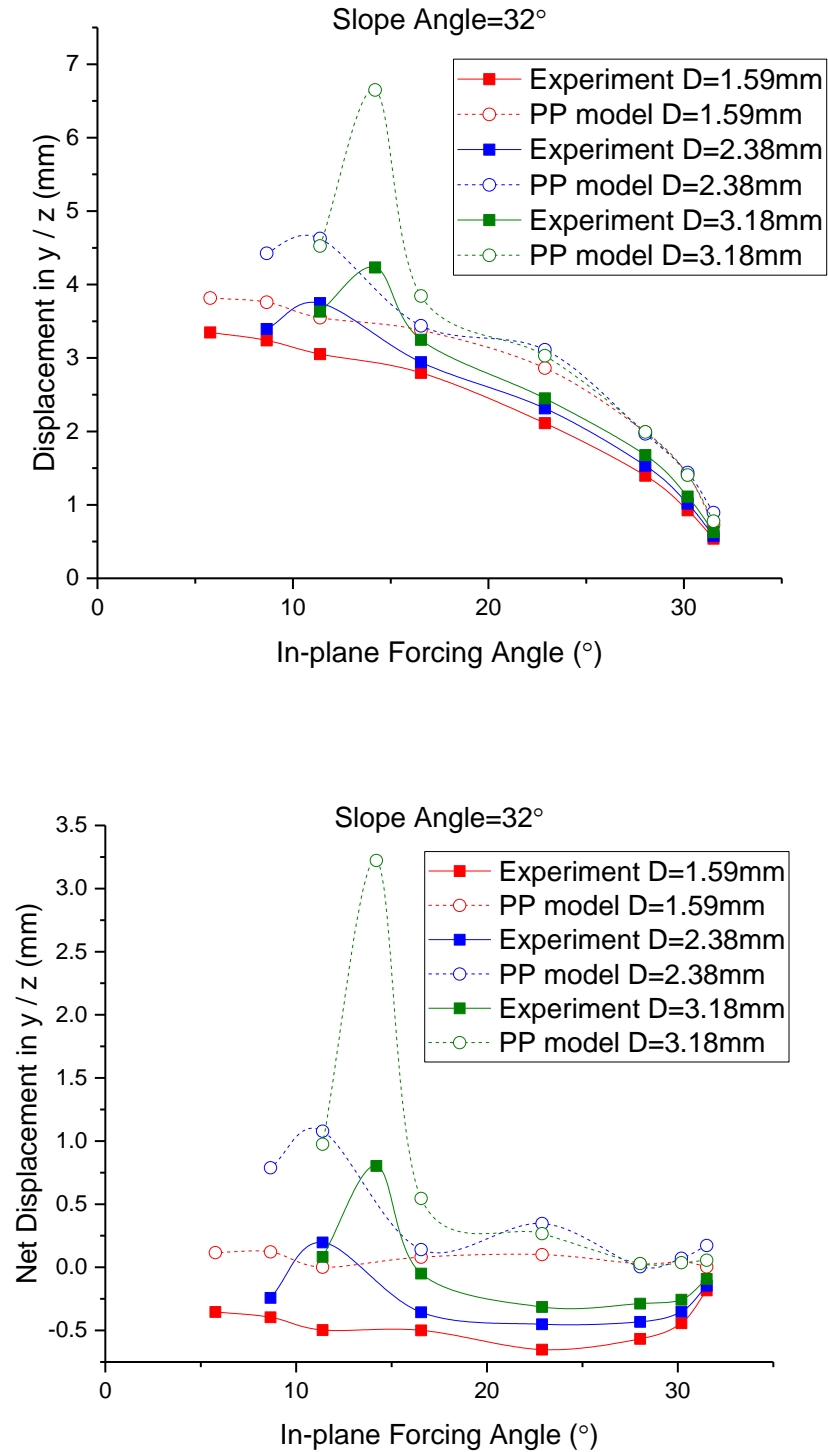


Figure 17. Longitudinal displacement per post in z direction of different sizes of particles when slope angle is 20.5° (a) and 32° (c). Net longitudinal displacement per post in z direction of different sizes of particles when slope angle is 20.5° (b) and 32° (d).

In experiments, critical angle is obtained by analyzing the transition pattern for each size of the particle. The critical offset is then calculated using geometry relation $b_c = l \sin \theta_c$. We investigate the existence of directional locking mode that the particle only moves along a column of post in z direction for forcing direction lower than a certain critical angle as 2D case. We also observe a peak value of longitudinal displacement near the critical angle which is because near transition angle where periodicity to be [0, 1]. Even though the periodicity of some angles are not exactly the same which may cause by the reasons that the critical offset got from experiment is an average value calculated by a range of critical angles, we can see that the point-particle model and experiment results have the same trend that the displacement in y increases with the rotation angle until getting a maximum value around critical angle. By comparing the net displacement per post, we find that at small rotation angles, there is little displacement which means that particles migrate following nearly the direction of the force field and that the migration path has significant change when the critical angle is reached. To separate these three sizes of particles, for example, if slope angle of 32° and rotation angle of 65° are chosen for the system, then for the of largest size of particles will have the longest distance displacement along obstacles and the smallest ones only move in the direction of the driving force thus we can separate them at one time. The discrepancy maybe caused by the assumption of the point particle model that the velocity along cylinder is always constant which actually is not the case in real.

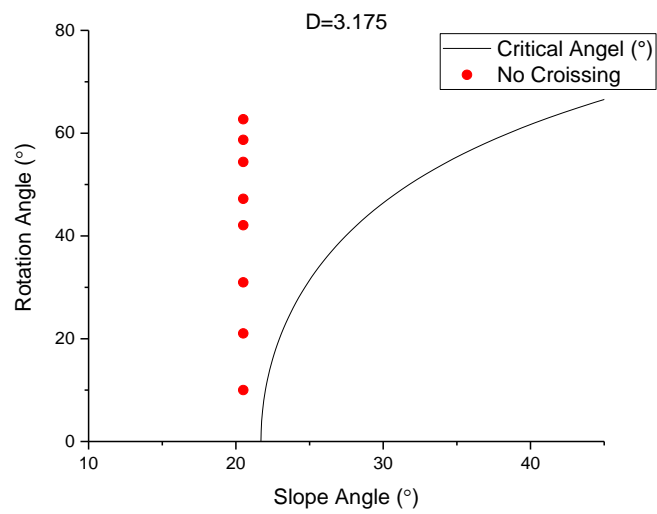
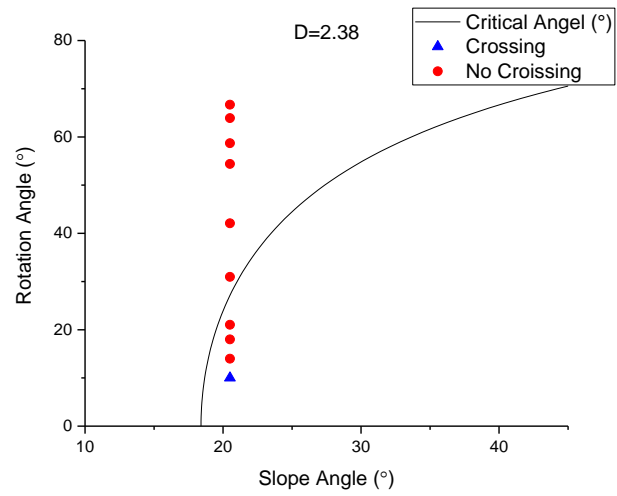
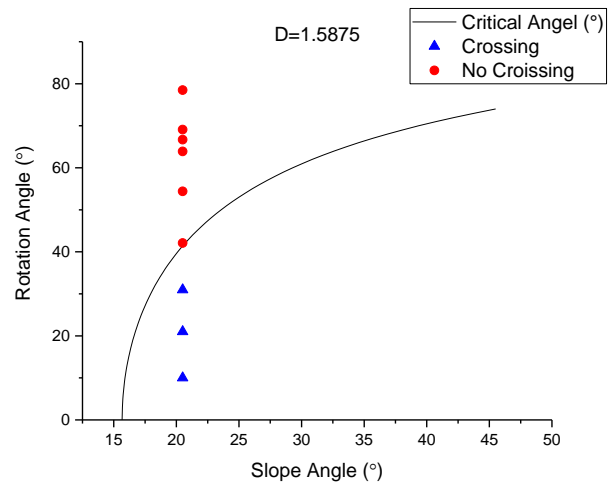
4.3 Comparison of point particle model with simulation

We simulate the particle moving pass multiple obstacles with a driving force added on the particle in quiescent fluid at zero Reynolds number and compared the results with point particle model where the critical offset b_c for different size of particles is from simulation of single particle-obstacle case by using same resolution and simulation box size. From simulation results for b_c , we see that the critical offset b_c increases with particle sizes (see Table 2).

Particle Size D	Critical Offset b_c	Theoretical Critical Angle α_c ($^\circ$)
1.5875	1.62	15.67
2.38	1.89	18.39
3.175	2.22	21.70

Table 2. Critical offset for three different sizes of particles single particle-obstacle simulation.

The theoretical transition angles are calculated by equation $\alpha_c = \arcsin(b_c/l)$ based on 2D model and the crossing type of periodicity is from simulation where [1,0] denotes that the particle only moves in the z direction and there is no crossing in the x direction which is the no crossing type trajectory. For the largest size of particle ($D=3.175$), only no crossing trajectory is observed for slope angle at 20.5° and decreasing particle sizes enables us to find a crossing. At same slope angle, the transition is found that for a smaller size of particle, a larger rotation angle is needed.



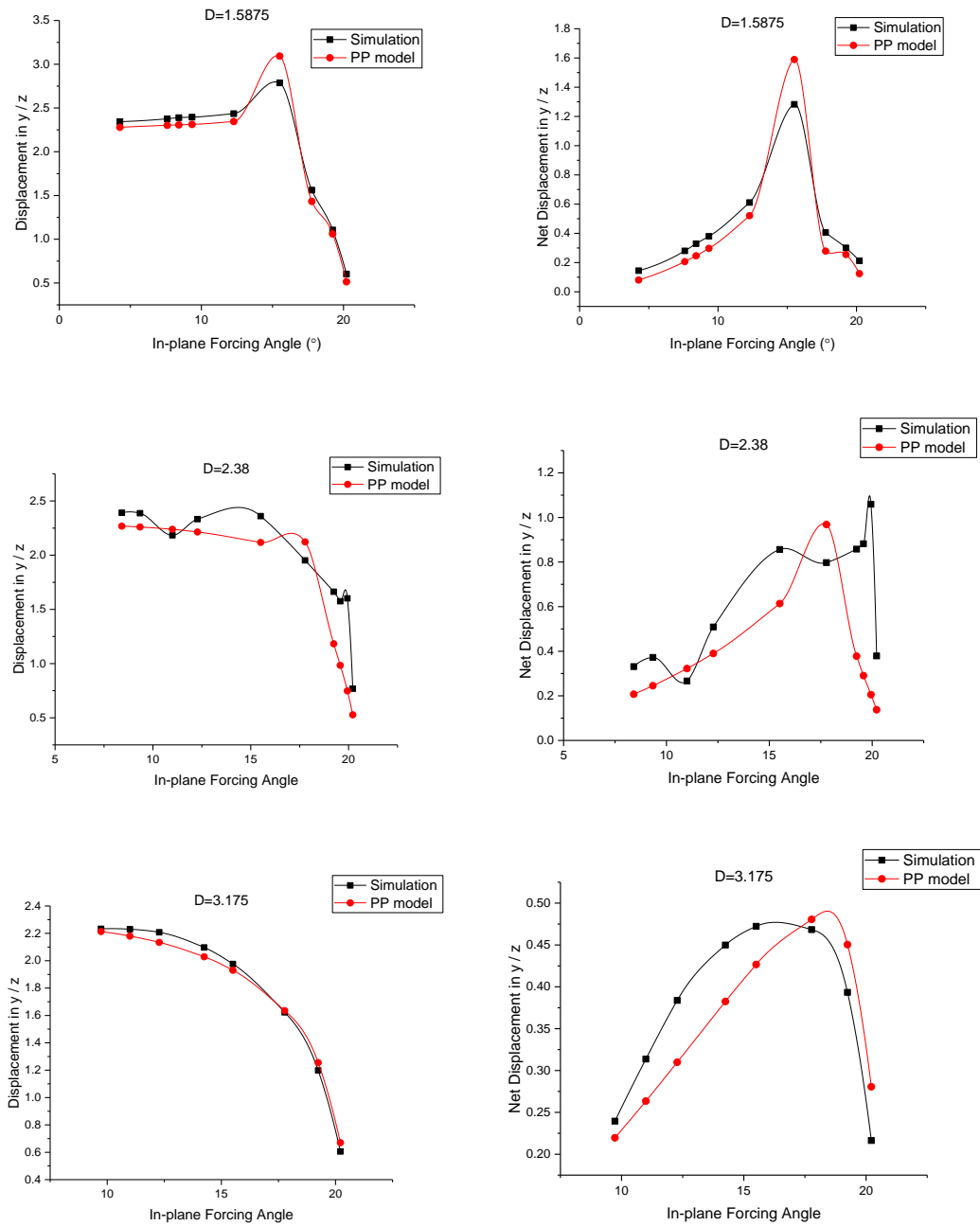


Figure 18. (a)-(c) Theoretical transition angle from 2D case with particle trajectory type from 3D. (d) Comparison of longitudinal displacement per periodicity for different sizes of particles from simulation with point-particle model.

We get a good agreement that transition happens near theoretical critical angles for particle size is 1.5875 and 3.175. While for the particle size of 2.38, the transition is smaller

than the theoretical results. At same slope angle, increasing the rotation angle gives an increasing trend on longitudinal displacement for different sizes of particles. For particle size $D=3.175$, no transition is observed for the whole range of rotation angles when slope angle is 20.5° and the displacement in y increases with rotation angle. For the other two sizes of particles, the peak values are found near the transition angle where crossing to no crossing occurs.

4.4 Triple separation

We present a method to separate three different sizes of particles simultaneously by choosing an optimal in-plane forcing angle. In Figure 19, point-particle model is used to calculate the periodicity and longitudinal displacement per z post by knowing the critical offset of these three sizes of particles from experiment. If we choose forcing angle equals to 12° , which is an angle between the critical angles of two larger sizes of parties, for the particle with size 3.175mm is separated from the other to by a no crossing type trajectory. For $D=1.5875\text{mm}$ and $D=2.38\text{mm}$, they move in the same periodicity trajectory which cannot be divided by in-plane motion. Then we use their out-of-plane motion to achieve separation. From Figure 19b, we find that 12° is angle near the critical angle of the medium size of particle and the longitudinal displacement at this angle has a maximum value. Based on their discrepancy in longitudinal displacement, the medium size of particle will displace more along the post so that these two sizes can be separated.

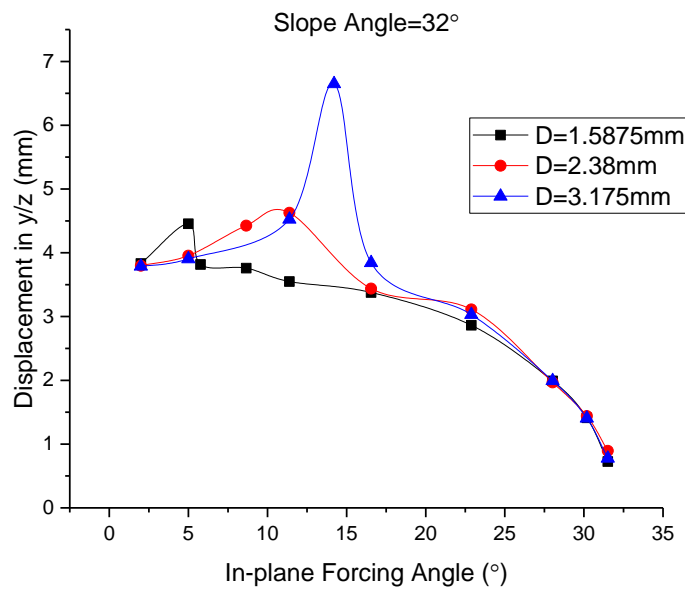
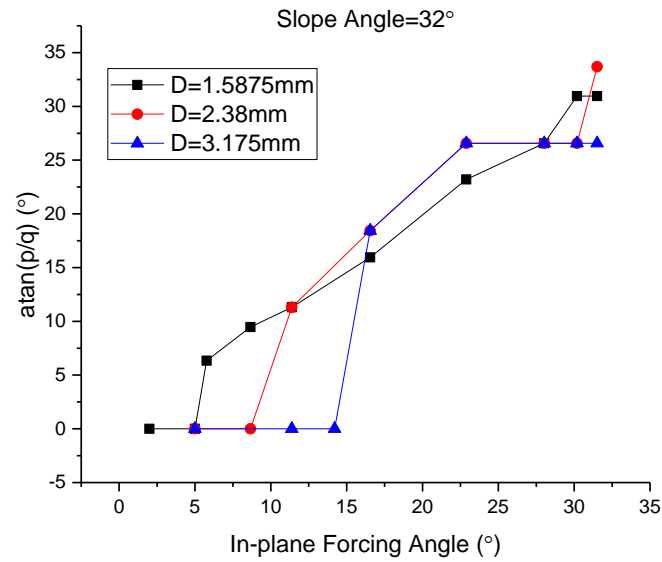


Figure 19. In-plane motion (a) and out-of-plane (b) motion for three different sizes of particles (1.5875mm, 2.38mm, 3.175mm) using point-particle model.

By applying both lateral and longitudinal displacement, we can achieve multiple sizes separation more efficiently comparing to the 2D-DLD by only choosing one optimal forcing direction.

5. Conclusions

We perform a mathematical 3D model and simulation to study the transport of suspended particles under uniform driving force or velocity field in quiescent fluid and find that the 3D system has the same directional locking mode as 2D-DLD devices. Also, a displacement in the direction along obstacles is observed. In the obstacle array, the crossing transition occurs near the critical angle and the displacement at critical angle is the largest compared with other angles. When the forcing angle is lower than the critical angle, the particle moves in the column of obstacles only in z direction which is the no crossing type trajectory. When this angle is beyond the critical angle, the crossing trajectory shows periodicity mode and the projection of the trajectory on the perpendicular plane of cylinder direction coincide with 2D case where there is no force applied along y direction. With two angles, the rotation and slope angles, we are able to find an optimal choice to separate different sizes particles using one obstacle array by crossing, no crossing of obstacles and different displacements based on particle sizes theoretically. The crossing and no crossing occurs at increasing rotation angles at same slope angles for larger particles enables particle separation. The lateral and longitudinal displacement is studied in the thesis both in experiment and simulation to help us better understand the mechanics of the 3D separation system. In 2D-DLD for multiple particles separation, different sizes of particles may have same lateral displacement which needed to be separated twice. Using this 3D model, we can separate particles using lateral displacement and longitudinal displacement at one time for a certain rotation and slope angle which provide us a more efficient separation method.

Reference

1. Sajeesh, P. & Sen, A. K. Particle separation and sorting in microfluidic devices: a review. *Microfluid. Nanofluidics* 17, 1–52 (2013).
2. Gascoyne, P. R. C. & Vykoukal, J. Particle separation by dielectrophoresis. *Electrophoresis* 23, 1973–1983 (2002).
3. Miltenyi, S., Müller, W., Weichel, W. & Radbruch, A. High gradient magnetic cell separation with MACS. *Cytometry* 11, 231–238 (1990).
4. MacDonald, M. P., Spalding, G. C. & Dholakia, K. Microfluidic sorting in an optical lattice. *Nature* 426, 421–424 (2003).
5. Laurell, T., Petersson, F. & Nilsson, A. Chip integrated strategies for acoustic separation and manipulation of cells and particles. *Chem. Soc. Rev.* 36, 492–506 (2007).
6. Yamada, M., Nakashima, M. & Seki, M. Pinched Flow Fractionation: Continuous Size Separation of Particles Utilizing a Laminar Flow Profile in a Pinched Microchannel. *Anal. Chem.* 76, 5465–5471 (2004).
7. Hsu, C.-H., Carlo, D. D., Chen, C., Irimia, D. & Toner, M. Microvortex for focusing, guiding and sorting of particles. *Lab. Chip* 8, 2128–2134 (2008).
8. Bhardwaj, P., Bagdi, P. & Sen, A. K. Microfluidic device based on a micro-hydrocyclone for particle–liquid separation. *Lab. Chip* 11, 4012–4021 (2011).
9. Huang, L. R., Cox, E. C., Austin, R. H. & Sturm, J. C. Continuous Particle Separation Through Deterministic Lateral Displacement. *Science* 304, 987–990 (2004).
10. Collins, D. J., Alan, T. & Neild, A. Particle separation using virtual deterministic lateral displacement (vDLD). *Lab. Chip* 14, 1595–1603 (2014).
11. Hanasoge, S., Devendra, R., Diez, J. F. & Drazer, G. Electrokinetically-driven deterministic lateral displacement for particle separation in microfluidic devices. *ArXiv14054564 Cond-Mat Physicsphysics* (2014).
12. Beech, J. P., Holm, S. H., Adolfsson, K. & Tegenfeldt, J. O. Sorting cells by size, shape and deformability. *Lab. Chip* 12, 1048–1051 (2012).
13. Zeming, K. K., Ranjan, S. & Zhang, Y. Rotational separation of non-spherical bioparticles using I-shaped pillar arrays in a microfluidic device. *Nat. Commun.* 4, 1625 (2013).
14. Ye, S., Shao, X., Yu, Z. & Yu, W. Effects of the particle deformability on the critical separation diameter in the deterministic lateral displacement device. *J. Fluid Mech.* 743, 60–74 (2014).
15. Kulrattanarak, T., Sman, R. G. M. van der, Schroën, C. G. P. H. & Boom, R. M. Analysis of mixed motion in deterministic ratchets via experiment and particle simulation. *Microfluid. Nanofluidics* 10, 843–853 (2010).
16. D’Avino, G. Non-Newtonian deterministic lateral displacement separator: theory and simulations. *Rheol. Acta* 52, 221–236 (2013).
17. Devendra, R. & Drazer, G. Gravity Driven Deterministic Lateral Displacement for Particle Separation in Microfluidic Devices. *Anal. Chem.* 84, 10621–10627 (2012).
18. Bowman, T., Frechette, J. & Drazer, G. Force driven separation of drops by deterministic lateral displacement. *Lab. Chip* 12, 2903 (2012).
19. Devendra, R. & Drazer, G. Deterministic fractionation of binary suspensions moving past a line of microposts. *Microfluid. Nanofluidics* 17, 519–526 (2014).

20. Du, S. & Drazer, G. Deterministic separation of suspended particles in a reconfigurable obstacle array. *J. Micromechanics Microengineering* 25, 114002 (2015).
21. Balvin, M., Sohn, E., Iracki, T., Drazer, G. & Frechette, J. Directional Locking and the Role of Irreversible Interactions in Deterministic Hydrodynamics Separations in Microfluidic Devices. *Phys. Rev. Lett.* 103, 078301 (2009).
22. H.A. Stone, A.D. Stroock & Ajdari, A. Engineering Flows in Small Devices. *Annu. Rev. Fluid Mech.* 36, 381–411 (2004).
23. Frechette, J. & Drazer, G. Directional locking and deterministic separation in periodic arrays. *J. Fluid Mech.* 627, 379–401 (2009).
24. Koplik, J. & Drazer, G. Nanoscale simulations of directional locking. *Phys. Fluids 1994-Present* 22, 052005 (2010).
25. Risbud, S. R. & Drazer, G. Directional locking in deterministic lateral displacement microfluidic separation systems. *Phys. Rev. E* 90, (2014).
26. NITSCHKE, J. M. On Brownian Dynamics with Hydrodynamic Wall Effects: A Problem in Diffusion Near a Fiber, and the Meaning of the No-Flux Boundary Condition. *Chem. Eng. Commun.* 148-150, 623–651 (1996).